Synthesis and Characterization of Colloidal $CuInS_2$ Nanoparticles from a Molecular Single-Source Precursor

Stephanie L. Castro,*,† Sheila G. Bailey,‡ Ryne P. Raffaelle,§ Kulbinder K. Banger,† and Aloysius F. Hepp‡

Ohio Aerospace Institute, Cleveland, Ohio 44142, Photovoltaics and Space Environments Branch, NASA Glenn Research Center, Cleveland, Ohio 44135, and Department of Physics, Rochester Institute of Technology, Rochester, New York 14623

Received: February 27, 2004; In Final Form: April 15, 2004

Thermal decomposition of the molecular single-source precursor $(PPh_3)_2CuIn(SEt)_4$ in the presence of hexanethiol in dioctylphthalate forms colloidal $CuInS_2$ at 200 °C. The colloidal solution displays size-dependent quantum confinement behavior in the absorption and photoluminescence spectra. The average size of the nanocrystals can be increased from 2 to 4 nm by raising the reaction temperature from 200 °C to 250 °C. The nanoparticles are capped with hexanethiol ligands; these ligands can be exchanged with trioctylphosphine oxide or pyridine. The nature of the surface-capping ligands has a significant effect on the photoluminescence emission intensity. Investigation of the effect of synthesis parameters and postsynthesis treatments on the optical properties of the nanocrystals leads to the conclusion that the room-temperature emission originates in donor−acceptor defects.

Introduction

Chalcopyrite-based photovoltaic devices ($Cu(In:Ga)(S:Se)_2$) have been a focus of the space photovoltaic community for over two decades.[1−3] Thin-film photovoltaic devices made with chalcopyrite semiconductors are expected to be highly efficient. Thin-film $CuInS_2$ cells with efficiencies of 12.5% have been successfully produced,[4] and efficiencies up to 18.8% have been recorded for $Cu(In:Ga)Se_2$-based cells.[5] The band gaps of the ternary and quaternary chalcopyrite materials range from 1.5 eV ($CuInS_2$) to 1.1 eV ($CuInSe_2$) and are well matched to the AM0 solar spectrum. In addition, other materials properties such as high absorption coefficients, structural defect tolerance, and low-cost methods for deposition of thin films make these promising materials for photovoltaic devices.

As researchers search for ways to improve device performance, they are looking to new approaches, such as the use of nanotechnology, to meet their goals. Future photovoltaic devices may employ materials such as semiconductor quantum dots. Quantum dots are nanometer-sized particles whose small size allows for three-dimensional size-confinement of the bulk energy bands into discrete, molecular-like energy states. In this size regime, the band gap of a material can be "tuned" to a desired energy by adjusting the particle size, offering the possibility of growing quantum dots to match a specific region of the solar spectrum. The inclusion of nanocrystalline materials in photovoltaic devices[6] has been proposed to improve the efficiency of photon conversion (intermediate band solar cell),[7−10] as well as provide sites for exciton dissociation and pathways for electron transport.[11−16] Luque and Martí[7] proposed an Intermediate Band Solar Cell (IBSC) with a theoretical efficiency of over 63%, well in excess of the most efficient cells available today. New calculations by Brown et al.[10] increased the number of intermediate bands in the Luque model from one to two, and found a concomitant increase in efficiency to 71.7%. Composites of quantum dots and conductive organic polymers[11,12,16] have been employed to overcome some of the limitations of charge transport efficiency due to low electron mobility in conjugated organic polymers. Quantum dots are also more resistant to degradation from electron, proton, and alpha particle radiation than the corresponding bulk material, preferred characteristics for use in space solar cells.[17−19]

The possibilities of increased efficiency and resistance to radiation-induced defects led us to investigate quantum dots as part of our ongoing research on chalcopyrite materials for space photovoltaic applications. In contrast to the overall quantity of quantum dot research[20] in the literature, relatively few reports[21−29] have been published about the synthesis of nanosized I−III−VI_2 ternary materials $CuInS_2$ and $CuInSe_2$.

Colloidal synthesis of nanoparticles offers greater control over morphology and size than do MOCVD methods, particularly for very small particles. In the past decade, synthetic control over colloidal nanoparticles has greatly improved, especially for the II−VI and III−V semiconductors.[30] Recent work by O'Brien[31] and Strouse[32] with single-source precursors has shown them to be viable starting materials for the synthesis of high-quality colloidal quantum dots. Single-source precursors are discrete molecules that include all the elements required in the final material. These precursors can be designed with many properties in mind, including stoichiometry, solubility, and volatility. Our group has studied the synthesis of single-source precursors to $CuInS_2$ and $CuInSe_2$, and the subsequent conversion of these precursors to thin-films of the bulk semiconducting materials.[33−36]

In this study, $(PPh_3)_2CuIn(SEt)_4$[37]was used in the synthesis of colloidal $CuInS_2$ nanoparticles. In a previous study, we demonstrated the conversion of this precursor to insoluble

* Corresponding author: Stephanie Castro. c/o NASA Glenn Research Center, Mail Stop 302-1, 21000 Brookpark Rd. Cleveland, OH 44135. E-mail: stephanie.castro@grc.nasa.gov.
† Ohio Aerospace Institute.
‡ NASA Glenn Research Center.
§ Rochester Institute of Technology.

10.1021/jp049107p CCC: $27.50
Published on Web 07/27/2004

aggregates of nanocrystalline $CuInS_2$.[38] By modification of the surface with alkyl groups during synthesis, soluble colloids can be formed. The surface ligands can be exchanged in a post-processing step with any Lewis base; the bonding strength of the ligand influences the fluorescence efficiency. Here we report new methods of synthesis that lead to soluble colloidal $CuInS_2$. We examine the surface chemistry and solution optical properties of colloidal $CuInS_2$ prepared under different conditions.

Experimental Section

Materials. $(PPh_3)_2CuIn(SEt)_4$ was prepared by literature methods.[33d] The starting materials are slightly air sensitive and are stored in an argon-filled inert atmosphere drybox (Vac Atmospheres) to prevent decomposition. Standard air-sensitive (Schlenk) techniques were employed during synthesis. Dioctyl phthalate (DOP) (99+ %) was purchased from ACROS. Hexanethiol (95%), trioctylphosphine oxide (TOPO, 90%), pyridine (99%) and sulforhodamine B were purchased from Aldrich. Methanol (Optima grade), toluene (HPLC grade), hexanes (HPLC grade), and acetone (GR grade) were purchased from Fisher Scientific. All reagents were used without further purification.

Measurement. Optical absorption spectra were recorded on a Perkin-Elmer Lambda 19 spectrophotometer. Photoluminescence spectra were recorded on a Spex Fluoromax-3 spectrofluorometer. Solutions were placed in 1-cm quartz cuvettes for measurement. Fluorescence quantum yields were measured versus a sulforhodamine B solution in ethanol at an excitation wavelength of 510 nm. The absorbance of all solutions was maintained below 0.1 au at this wavelength to avoid internal filter effects. Elemental analysis (ICP−OES) was obtained from Galbraith Laboratories, Knoxville, TN. High-resolution transmission electron microscopy (HRTEM) was performed on a Philips CM200 operating at 200 kV in bright field mode. The digital image was collected on a Gatan Imaging Filter (GIF 1 k × 1 k). The magnification was calibrated using the Mag*i*cal TEM standard (http://www.emsdiasum.com/ems/calibration/magical.html). The TEM grids were Ted Pella 01881 lacey carbon; samples were prepared by dipping the grid into a milliliter of methanol containing suspended nanocrystalline powder and allowing the methanol to evaporate (insoluble samples) or by dipping the grid into a toluene solution of colloidal nanocrystals and allowing the toluene to evaporate (soluble samples). Powder X-ray diffraction (XRD) patterns were obtained on a Philips X′Pert diffractometer using Cu Kα radiation, excited at 45 kV and 40 mA. The X-rays were collimated at the source with a 10-mm mask and divergence slit set at 1°, and at the detector with a 2-mm receiving slit and anti-scatter slit set to 1°.

Preparation of $CuInS_2$ Nanoparticles

Sample **1**. Dioctyl phthalate (30 mL) was heated to 125 °C under vacuum for 1 h to dry and degas the solvent; the flask was backfilled with argon and cooled to room temperature prior to adding the precursor. $(PPh_3)_2CuIn(SEt)_4$ (1.5 g, 1.6 mmol) was added to the reaction flask and heating resumed. At approximately 150 °C the precursor dissolved to form a transparent yellow solution; no further change was observed with time at this temperature. At this point, the solution could be returned to room temperature without reprecipitation of the precursor. The yellow color is likely due to a trace amount of decomposition or impurity; the absorption spectrum of the yellow dioctyl phthalate solution is indistinguishable from that of a toluene solution of the precursor. In addition, the precursor can be recovered in near-quantitative yield by addition of hexanes to the yellow dioctyl phthalate solution. At 150 °C, the precursor remains, for the most part, intact. The solution was then cooled to 100 °C, hexanethiol (3 mL, 21 mmol) was added, and the temperature was raised to the 200 °C and held for 5 h. The solution became deep red-orange in color. After cooling to room temperature under argon, the product is isolated by precipitation with methanol and was dried under vacuum at 60 °C. The washing and centrifugation steps were carried out in air. The product is only slightly air-sensitive at room temperature; a green tinge was observed on the surface of the powder after several weeks' exposure to air and room light. An amount (0.472 g) of **1** was collected and stored in a glovebox. Elemental analysis for copper and indium gave Cu: 15.71% w/w and In 30.64% w/w, or a 1:1.08 atomic ratio. Sulfur is present in a Cu:S ratio of 1:2.84. An excess of sulfur is expected due to the thiol ligands on the surface of the nanocrystals.

Sample **2** was synthesized by the same method at 225 °C for 2 h. A brown oil was isolated by addition of MeOH; the product was extracted with hexanes and precipitated with acetone to produce a powder.

Sample **3** was synthesized by the same method at 250 °C for 2 h. The product was not soluble in organic solvents; the black powder obtained was washed sequentially with hexanes, toluene, and methanol, then dried under vacuum.

Size-focusing Methods[39] were applied to the synthesis of nanocrystalline $CuInS_2$. In this method, "seeds" of nanocrystals are formed at the appropriate nucleation temperature. When the concentration of available precursor is no longer sufficient to support nanocrystal growth, additional precursor reagents are added at a temperature below that which would cause new seeds to nucleate. The new precursor adds to the existing seeds, growing them larger while at the same time focusing the size distribution. This method has been successfully applied to II−VI, III−V,[39] and III−VI[40] colloidal systems. With heating in 5 ml of DOP, 500 mg of $(PPh_3)_2CuIn(SEt)_4$ was dissolved, and then withdrawn into a syringe. In a separate flask, an additional 5 mL of DOP and 1 mL hexanethiol were degassed and heated to 200 °C. Then, 2.5 mL of the precursor solution was injected quickly into the hot DOP and the temperature maintained at 200 °C for 2 h. An aliquot of the solution was removed at this time for spectroscopy. The temperature was then lowered to 190 °C, which is below the nucleation temperature of the nanocrystals, and the remainder of the precursor solution added. The temperature was maintained at 190 °C for 1 h, with aliquots removed every 15 min. The temperature was finally raised to 200 °C for 1 h. The solution was cooled under argon flow and the product precipitated with methanol and extracted with hexanes. The aliquots were precipitated with methanol and redissolved in toluene for spectroscopy.

Size-selective Precipitation[41] was performed on toluene solutions of the nanocrystals. In this way, the largest nanocrystals are preferentially removed from the solution, leaving the smaller fraction suspended. Methanol was added dropwise to a toluene solution containing a few milligrams of **2** until a precipitate just began to form. The mixture was centrifuged and the supernatant decanted. The solid pellet was redissolved in toluene for spectroscopy. The process was repeated with the supernatant until ten samples were obtained.

Surface Modification of $CuInS_2$ nanocrystals. To examine the effects of the surface ligands on the optical properties of the nanocrystals, the hexanethiol ligands were replaced with TOPO and with pyridine. To exchange with TOPO, 1 mL of a

hexanes solution containing a few milligrams of **2** was placed in a flask with 0.5 g TOPO and heated to 100 °C under vacuum until the hexanes were evaporated, then backfilled with argon and maintained at 60 °C overnight. After cooling to room temperature, the resulting solid was washed with methanol to remove excess TOPO and then dissolved in 2 mL toluene. A small amount of undissolved material was removed by centrifugation. Successful removal of hexanethiol was confirmed by repeating this procedure on a larger scale and isolating the hexanethiol in a liquid nitrogen trap during the vacuum/heating stage.

To exchange with pyridine, 3 mL of pyridine was added to a flask containing 1 mL of a hexanes solution containing a few milligrams of **2**. After 24 h, the nanocrystals were precipitated by addition of more hexanes, centrifuged, and the resulting solid dissolved in chloroform.

Results

General. The single-source precursor $(PPh_3)_2CuIn(SEt)_4$ decomposes at temperatures above 200 °C to form the ternary compound semiconductor $CuInS_2$. When alkanethiols are present in the reaction mixture, the $CuInS_2$ forms as a nanocrystalline colloid. Absence of a coordinating ligand leads to the formation of aggregated nanocrystals.[38] Successful colloid formation depends on the presence of thiols. Unlike, for example, CdSe colloids, ligands such as phosphine oxides,[41] carboxylic acids,[42] or amines[43] could not be added to the reaction mixture. TOPO, trioctylphosphine, oleic acid, stearic acid, hexadecylamine, and combinations of these commonly employed ligands lead to the formation of aggregated materials with varying (including none) amounts of indium that are detected by energy dispersive spectroscopy. In the case of TOPO, crystalline copper sulfides were isolated. We hypothesize that these other ligands have significantly different bonding affinities for the two metals and therefore inhibit stoichiometric incorporation of the metals into the final product. The alkanethiol-coated nanocrystals are readily dispersible in nonpolar organic solvents such as hexanes and toluene; they are precipitated by polar organic solvents such as methanol, acetonitrile, and acetone. Once formed, the surface ligands can be exchanged by incubating the nanocrystals in an excess of the desired new ligand.

The absorption spectra of nanocrystal solutions show a broad shoulder with a long tail to lower energies, both significantly shifted from the bulk band-gap absorption of $CuInS_2$ (1.55 eV). Shown in Figure 1 are typical absorption, emission, and photoluminescent excitation spectra for solutions of $CuInS_2$ colloidal nanocrystals.

Two peaks can be located in the second derivative absorption and emission spectra; in some samples a third, smaller peak is found as well. The ratio of the two main peaks in the emission spectrum varies considerably with sample synthesis and storage. For a given sample, the ratio of the higher and lower energy peaks was found to change after storage of the solid material for 6 months in an argon-filled glovebox in a clear glass vial, compared to a sample stored in air for 3 months in an amber vial. The peak positions, however, did not change significantly. These spectra are typical for the product regardless of the temperature at which the precursor was added to the reaction mixture. The same results are observed for reactions in which the precursor is dissolved in DOP and injected into a second flask of DOP at 300 °C. The "high-temperature injection" method is more typical for colloidal nanocrystal syntheses and is sometimes required to produce narrow size distributions. However, this method did not narrow the width of the peaks in the absorption or emission spectra.

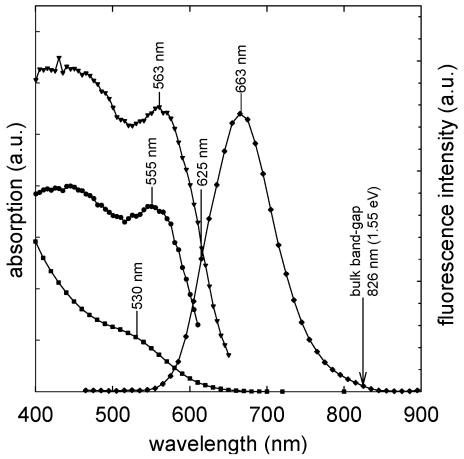

Figure 1. Absorption (filled squares), fluorescence emission (filled diamonds), and photoluminescent excitation (at 663 nm, filled triangles and 625 nm, filled circles) spectra of a typical colloidal solution of $CuInS_2$ (hexanethiol) nanocrystals.

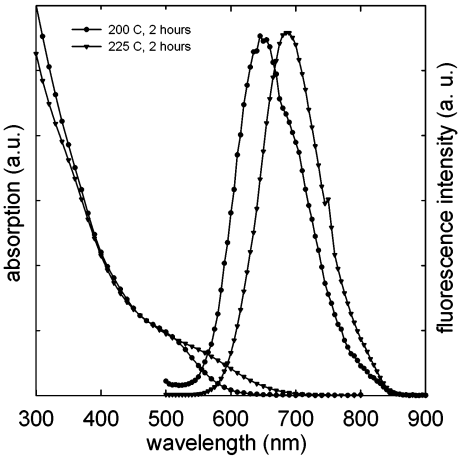

Figure 2. Absorption and fluorescence emission spectra of $CuInS_2$ (hexanethiol) samples grown at 200 (filled circles) and 225 °C (filled triangles), respectively. The intensities of the spectra have been normalized to arbitrary values for comparison.

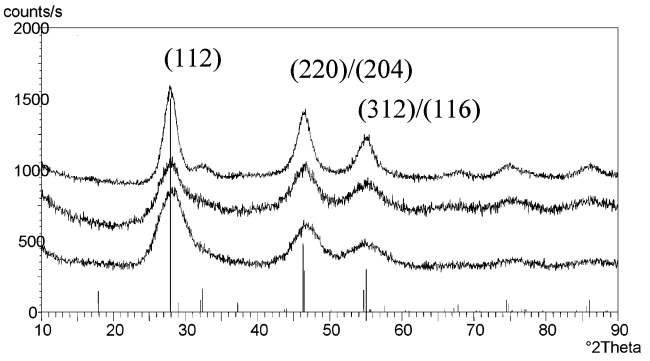

Figure 3. Powder X-ray diffraction patterns for $CuInS_2$ samples synthesized at 200 °C (bottom), 225 °C (center), and 250 °C (top). Reference pattern 85−1575 ($CuInS_2$) is shown along the *x*-axis for comparison.

Effect of Growth Temperature. As shown in Figure 2, the energy of the absorption peak shifts to lower energy when the nanocrystals are grown at higher temperature, indicating larger average nanocrystal sizes.

The effect of temperature upon nanocrystal size is also evident in the X-ray diffraction patterns, as shown in Figure 3. The XRD peaks are progressively narrower at higher synthesis temperatures, indicating larger particle sizes, as described by

the Scherrer formula. Using the Scherrer formula, the diameters of the nanocrystals are calculated to be: 2.1 ± 0.2 nm at 200 °C, 2.7 ± 0.3 nm at 225 °C, and 4.0 ± 0.1 nm at 250 °C. The error is calculated by averaging the sizes obtained using both the (112) and (220) diffraction lines; the presence of overlapping lines in the diffraction pattern makes the use of the Scherrer formula only an estimate for this compound. Regardless, the data show a clear trend to narrower diffraction lines, and hence larger nanocrystals, at higher synthesis temperatures.

TEM is also employed to determine the particle size. Figure 4 shows TEM images of nanocrystals grown at 200, 225, and 250 °C, respectively. While we were unable to obtain high-resolution images of the nanocrystals grown at 200 °C, it is clear from the TEM image that the nanocrystals are small (~2 nm diameter), with some larger nanocrystals present. At 225 °C, the nanocrystals measure 2.68 nm on average, which is in good agreement with the value of 2.7 determined by the Scherrer formula. At 250 °C, the nanocrystals measure 3.35 nm, with a standard deviation of 0.88 nm. This number also agrees within experimental error to the size determined by XRD. Clearly, the nanocrystal size is influenced by growth temperature.

Optical Properties. The lack of a distinct exciton peak in the absorption spectrum coupled with a long tail on the low energy side could be the result of several factors, alone or in combination with each other. First, it could be indicative of a very poor size distribution. Several methods (high-temperature injection, size focusing, and size selective precipitation) were employed to improve the size distribution of the sample. Second, it could be a result of electron density leakage from the core of the nanocrystals into the organic ligand layer. Ligand substitution experiments were employed to investigate this possibility. Third, it could be the result of intraband gap states.

Size-focusing experiments (vide supra) were performed to attempt to narrow the size distribution of the product. There was no change in the position of the lowest energy peak (usually associated with an excitonic transition and an indicator of nanocrystal size) after additional precursor solution is added to the nanocrystals "seeds". The emission spectra were also unaffected. This is the opposite of what has been observed for CdSe solutions.[39] After a secondary injection of CdSe precursors, there is an increase in nanocrystal size accompanied by a decrease in the width of the emission peak. For the $CuInS_2$ colloids, only after the temperature was raised again to the "nucleation" temperature did the positions of the absorption and emission peaks change. No narrowing of the peaks occurred during this procedure. These results indicate that decomposition of the $CuInS_2$ precursor does not occur at temperatures below 200 °C, even in the presence of nanocrystal seeds. At 200 °C, the additional precursor then added to the existing seeds instead of forming new nanocrystals, increasing the average size of the nanocrystals. However, the size distribution of the nanocrystals was not improved by this procedure.

Size-selective precipitation can also improve the size distribution in a sample of nanocrystals. In this experiment, both UV−vis and fluorescence spectroscopy indicated that larger nanocrystals were sequentially removed from the solution during size-selective precipitation, as evidenced by a shift to higher energy in the absorption and fluorescence spectra. The position of the lowest energy peak (identified in the second derivative spectrum for each sample) moved to higher energy with each subsequent aliquot, indicative of the removal of the largest subset of nanocrystals from the solution. Thus, it is clear that there is some distribution of sizes present in the reaction product. However, the overall shape and width of the spectra did not

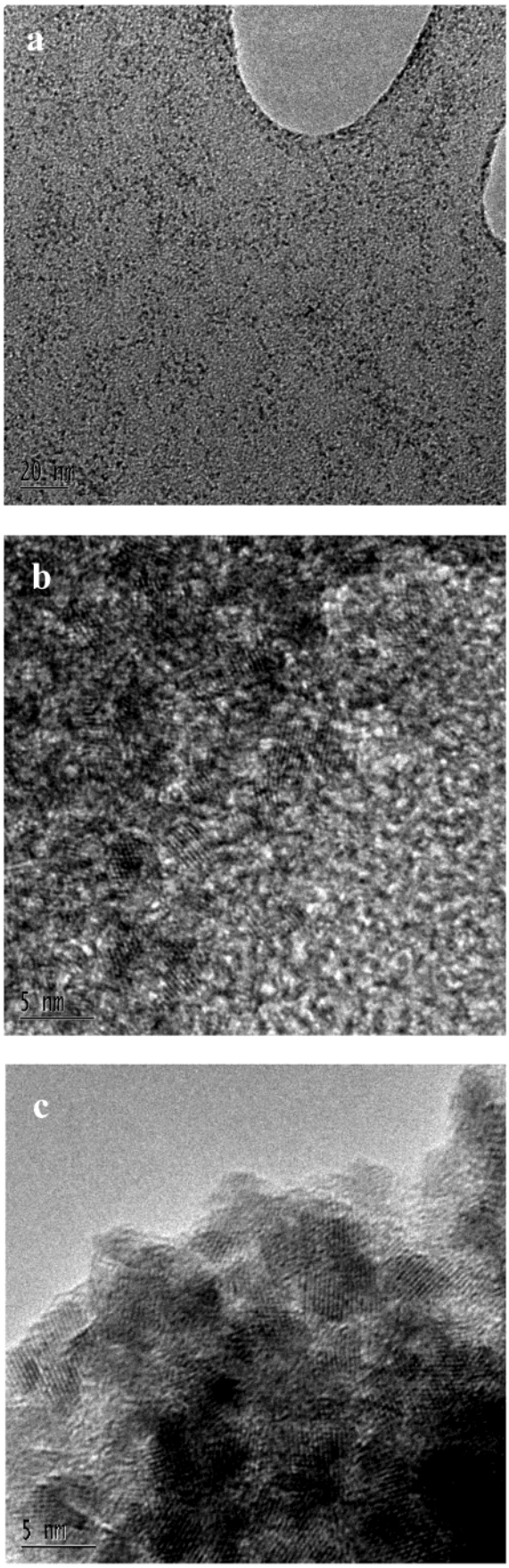

Figure 4. (a−c). TEM images of $CuInS_2$ nanocrystals grown at 200, 225, and 250 °C, respectively. Samples grown at 200 and 225 °C were evaporated on the TEM grid from toluene solution; the sample grown at 250 °C was suspended in methanol by sonication prior to deposition on the grid. Scale bars in the images are 20, 5, and 5 nm, respectively.

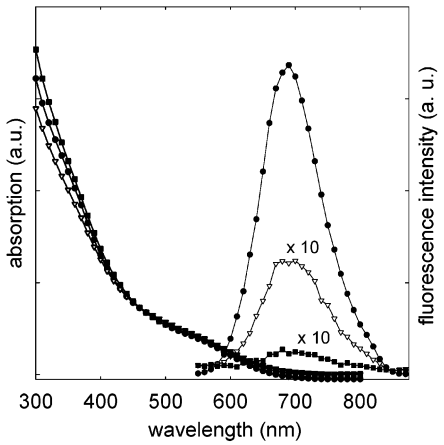

Figure 5. Absorption and fluorescence emission spectra of colloidal $CuInS_2$ with hexanethiol (filled circles), TOPO (empty triangles), and pyridine (filled squares) organic capping ligands.

change, as would be expected for size-distribution narrowing by selective precipitation. The full-width-half-maximum of the emission spectrum remained constant at 100 ± 5 nm, and the long red tail on the absorption onset shifted slightly to higher energy, but did not disappear. The shape of an excitonic emission spectrum for a sample containing a range of sizes would be expected to be broad, but symmetric, as the ensemble emission spectrum would be made up of the sum of the individual emission spectra.[44] The emission spectra of the $CuInS_2$ nanocrystals consistently display two to three peaks, regardless of synthetic conditions. While the presence of multiple distinct peaks could indicate a bimodal (or higher) size distribution, it is unlikely that such a range of synthesis conditions as has been employed here would consistently lead to such a situation. Also, the excitonic peak does not become more distinct in the absorption spectrum. These results indicate that although a size distribution of nanocrystals is present, the broad features in the absorption and emission spectra can be attributed *in part* to other factors. As shown by the size-selective precipitation experiments and observed in the TEM images, a size distribution of the nanocrystals is present in the product at all temperatures. If a broad size distribution is solely responsible for the width of an excitonic emission peak, size-selective precipitation should narrow the excitonic emission peak due to removal of larger nanocrystals absorbing and emitting at longer wavelengths. The independence of the width of the emission peak on the processing conditions supports the conclusion that size distribution is not the only source of the broad emission.

Surface Modification. To determine the effect of the surface ligands on the optical properties of the nanocrystals, three solutions were prepared for absorption and fluorescence spectroscopy. Hexanethiol-coated $CuInS_2$ in hexanes, TOPO-coated $CuInS_2$ in toluene, and pyridine-coated $CuInS_2$ in chloroform were diluted to have absorptions of <0.1 au at 510 nm. Absorption spectra were collected from 800 to 300 nm, and fluorescence emission spectra were collected from 520 to 900 nm. The solutions were excited at 510 nm, and the PL signal integrated from 550 to 850 nm. Fluorescence quantum yield for the solutions was calculated relative to a sulforhodamine B solution in ethanol. The spectra are shown in Figure 5 and the quantum yield, relative area, and *fwhm* are tabulated in Table 1.

The nature of the surface ligands plays an important role in the PL efficiency of $CuInS_2$ nanocrystals. As has been observed for CdSe nanocrystals, surface defects provide sites for charge trapping, leading to nonradiative recombination of the electron and hole and quenching of the fluorescence emission.[45] Passivation of these sites with a strong ligand, such as hexadecylamine[43] or a higher band-gap material such as ZnS[46] or CdS[47] leads to increased quantum yield, while a weak ligand such as pyridine further increases the quenching effect. Similar observations are made with $CuInS_2$, indicating that surface states on the nanocrystals play an important role in fluorescence. As can be seen in Figure 5, the nature of the surface ligands does not affect the shape of the absorption spectrum. From this it can be concluded that the broad onset of absorption is not due to participation of surface ligand electronic states. However, the photoluminescent efficiency is strongly affected by the nature of the surface ligands. A 179-fold decrease in emission intensity is observed by changing the surface ligands from hexanethiol to pyridine. This implies that the surface of the nanocrystals provides a significant source of defects or unpassivated sites where nonradiative recombination can take place.

TABLE 1: Effect of Surface Ligands on Fluorescence Emission Intensity of Colloidal $CuInS_2$

	hexanethiol	TOPO	pyridine
fwhm (nm)	109	107	113
area ratio	179	6.6	1
quantum yield	4.4%	0.16%	0.024%

Neither broad size distribution nor surface states alone can fully account for the appearance of the optical spectra of colloidal $CuInS_2$. We submit that the best explanation is the contribution of intraband gap states.

The photoluminescence of single-crystal $CuInS_2$ is complicated by the presence of intraband gap levels near the conduction and valence band edges. $CuInS_2$ has a complicated defect chemistry because of variation in molecularity ([Cu]/[In]) and stoichiometry ([S]/[Cu]). Examples of defects are copper and indium vacancies and interstitials, and excess or deficient sulfur occupancy. $CuInS_2$ can be prepared as either n- or p-type conductivity by varying the atomic ratios. High-quality crystalline material of both conductivity types displays narrow band-edge emission between 1.5 and 1.55 eV, consisting of up to 10 narrow lines.[48−50] These transitions arrive from recombination of free excitons, excitons bound to neutral or ionized donors and acceptors, and donor-valence band pairs; they are diagrammed in Figure 6.

Crystals with a high concentration of defects may not exhibit near-band edge luminescence at all, as screening of the discrete exciton states may occur.[50] Free exciton emissions (FE_A and FE_B) are the result of free exciton recombination with a binding energy of about 20 meV from the conduction band. They recombine with the Γ_6 or Γ_7 doubly degenerate valence bands. Γ_6 and Γ_7 are separated by $\sim$18 meV in energy as a result of spin−orbit interactions. The FE_B emission is only observed in p-type $CuInS_2$. Bound exciton (EX_1−EX_6) emission results from recombination of excitons bound to neutral or ionized donors or acceptors. Some of these lines have been assigned to specific states.[48,50] Donor-valence emission (DV) is observed in sulfur-deficient single crystals. It results from a recombination of an electron at a sulfur vacancy with the valence band. The donor state (D_1) is $\sim$35 meV below the conduction band. Near-edge emission is very sensitive to the defect chemistry and surface conditions of the $CuInS_2$ crystals and is not always observed, especially in less-than-perfect crystals. It is also extremely broadened at increasing temperature. These observations were made at <10 K.[48−50] To the best of our knowledge, room temperature near-edge emission has only been reported once.[48]

A second group of emission peaks is observed at lower energy (1.35−1.45 eV) and are termed broad-band emission.[51] Broad-

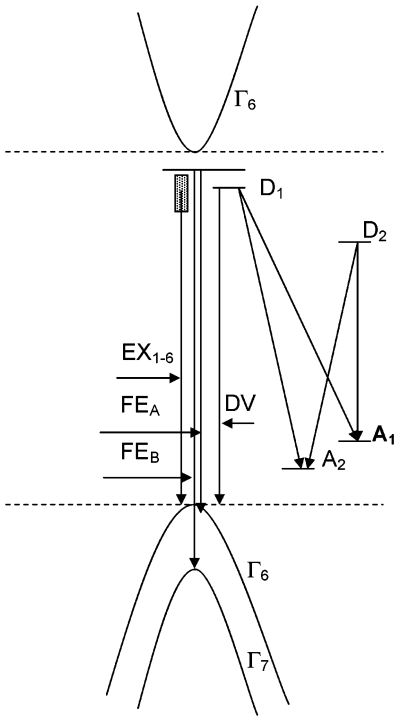

Figure 6. Schematic diagram of the energy levels and transitions that have been observed in single-crystal $CuInS_2$.

band emission is observed in nearly all samples of $CuInS_2$. The emission is characterized by two broad lines, separated by a constant energy from each other. Depending on the synthesis conditions, a very broad emission spectrum resulting from all four lines overlapping has been observed. Two donor states, D_1 and D_2, are found at energies of ~35 and 70 meV below the conduction band, resulting from a sulfur vacancy (D_1) and either an indium interstitial or copper−indium substitution (D_2) (assignment is tentative).[52] Electrons in these donor states can recombine with acceptor states A_1 (100 meV above the valence band, indium-rich samples only) or A_2 (150 meV above the valence band, copper-rich samples only).

Based on comparison to the single-crystal studies, we conclude that the origin of the emission in these nanocrystalline $CuInS_2$ samples is broad-band in nature. The distinguishing features support this claim. First, the large energy shift between the excitation and emission peaks is inconsistent with an excitonic process. In the example shown in Figure 1, the two peaks in the emission spectrum at 625 and 663 nm (1.98 and 1.87 eV) each contain a distinct peak in their PLE spectrum that is at a significantly higher energy (555 and 563 nm, or 2.23 and 2.20 eV). This is consistent with the donor−acceptor transitions in Figure 6. The peaks in the PLE spectrum also fall at lower energies than the peak in the absorption spectrum; they are in the broad tail region, supporting the assignment of the tail to intra-band gap transitions.

It could also be argued, however, that this is only evidence of a broad size distribution. Volume dominance of the largest nanocrystals in the sample would cause a large red shift in the emission relative to the global excitation peak while broadening the spectrum, and the absorption tail would be broadened as well. If this is so, the lowest energy peak in the PLE spectrum should shift to longer wavelengths as the emission wavelength is lengthened. Also, as the excitation wavelength is increased, the resulting emission spectrum should become narrower as a smaller subset of nanocrystals is excited. The PLE spectra of a sample whose global emission maximum was 660 nm (excitation at 475 nm) and has a *fwhm* of 100 nm were recorded at emission detection wavelengths varying from 600 to 750 nm. The first peak of the PLE spectrum does shift from 544 to 565 nm as the detection wavelength is varied from 600 to 660 nm, but then remains constant at 565 nm for detection wavelengths between 660 and 750 nm. A series of PL spectra were collected where the excitation wavelength was varied between 575 and 625 nm (this includes the entire absorption tail). The emission maximum shifts slightly, from 662 to 673 nm, but the *fwhm* remains constant at 100 nm. These two observations are in conflict with what would be expected for a sample suffering only from a poor size distribution.

Second, the emission is observed at room temperature. Near-edge excitonic emission has been observed only once at room temperature for single-crystal $CuInS_2$, and this was in a high-purity single crystal prepared at ~900 °C.[48] Even at low temperatures, the excitonic emissions are readily quenched in the presence of defects. Due to the low synthesis temperatures for the colloidal $CuInS_2$, it is likely that there are a great number of defects present in the nanocrystals. By virtue of the naturally small size of nanocrystals, defects could make up a far larger proportion of the total atomic volume than in macroscale samples.

The near-band edge and broad-band emission of $CuInS_2$ can sometimes be distinguished by the effect of varying the excitation energy on the energy and intensity of the emission lines.[51] For free exciton, bound exciton, and donor-valence emission, the emission energy is independent of the excitation intensity. However, the emission intensity (I) is proportional to power (P) in the relationship $I \sim P^{\alpha}_1$. For donor−acceptor (broad-band) emission, the emission energy is expected to increase with increasing excitation energy according to the equation $E_P = E_{P0} + \beta(\log P_1 - \log P_{10})$, where E_P and E_{P0} are the peak energies at powers P_1 and P_{10}, respectively, and β is the energy shift per decade shift in P_1. However, β decreases rapidly with increasing temperature, becoming <1 meV at 80 K, so at 300 K E_P is expected to be equal to E_{P0}. Further experiments at cryogenic temperatures are required to conclusively determine the effect of variable excitation energy on the emission of the nanocrystalline $CuInS_2$ and to more clearly distinguish the effects of size distribution on the spectra.

Based on the large energy difference between the absorption peak and the emission peak, the presence of multiple emission peaks, the fact that the ratio of these peaks is not constant between samples, and the observation of the PL at room temperature, it is concluded that the PL of the colloidal $CuInS_2$ presented here is broad-band, or donor−acceptor defect based, in nature. It is not surprising that $CuInS_2$ synthesized at a very low temperature would have many defects. It is difficult to grow bulk $CuInS_2$ that exhibits near-edge PL, and that material is usually synthesized at 700−900 °C.

Conclusions

We report here the first synthesis of colloidal ternary chalcopyrite nanoparticles from a single-source precursor. The method produces nanocrystals of $CuInS_2$ with sizes between 2 and 4 nanometers, with a controllable surface chemistry. Solutions of the nanocrystals fluoresce at room temperature, a property rarely observed in bulk samples. Examination of the absorption, emission, and photoluminescent excitation spectra lead to the conclusion that this fluorescence arises from intraband gap transitions. The optical properties of the nanocrystals are complicated by the presence of a size distribution that is not substantially narrowed by size-selective precipitation,

size focusing, or high-temperature injection methods. Future work will include measurement of the temperature- and excitation-intensity dependent nature of the emission to provide greater insight into the origin of the intraband gap states.

Acknowledgment. We thank David Hull of the NASA Glenn Research Center for the TEM images, and NASA Cooperative Agreements NCC3-958 (S.L.C.) and NCC3-947 (K.K.B.), NSF-JIETSSP (0233776) (S.L.C. and R.P.R.), and the NASA Energetics program (Glenn Research Center) for funding.

Supporting Information Available: Plots of absorption vs wavelength and emission intensity vs wavelength are available for experiments in size-focusing and size-selective precipitation (four graphs). This material is available free of charge via the Internet at http://pubs.acs.org.

References and Notes

(1) Bailey, S. G.; Flood, D. J. *Prog. Photovolt. Res. Appl.* **1998**, *6*, 1−14.

(2) Schock, H. W.; Noufi, R. *Prog. Photovolt. Res. Appl.* **2000**, *8*, 151−160.

(3) Schock, H. W.; Bogus, K. Development of CIS solar cells for space applications. In *Proceedings of the Second World Conference on Photovoltaic Energy*; Schmid, J., Ossenbrink, H. A., Helm, P., Ehmann, H., Dunlop, E. D., Eds.; EC Joint Research Center: Luxembourg, July 1998; 3586−3589.

(4) Klaer, J.; Bruns, J.; Henninger, R.; Töpper, K.; Klenk, R.; Ellmer, K.; Bräunig, D. A tolerant two step process for efficient $CuInS_2$ solar cells. In *Proceedings of the Second World conference on Photovoltaic Solar Energy Conversion*; Schmid, J., Ossenbrink, H. A., Helm, P., Ehmann, H., Dunlop, E. D., Eds.; EC Joint Research Center: Luxembourg, July 1998; 537−540.

(5) Contreras, M. A.; Egaas, B.; Ramanathan, K.; Hiltner, J.; Swartzlander, A.; Hasoon, F.; Noufi, R. *Prog. Photovolt. Res. Appl.* **1999**, *7*, 311−316.

(6) A collection of reviews on this topic is available in a special issue of *Physica E* (**2002**, *14*, issue 1−2) entitled "Nanostructures in Photovoltaics".

(7) (a) Luque, A.; Martí, A. *Phys. Rev. Lett*. **1997**, *78*, 5014−5017. (b) Martí, A.; Cuadra, L.; Luque, A. Quantum Dot Intermediate Band Solar Cell. In *Twenty-eighth IEEE Proceedings of the Photovoltaics Specialists Conference*, Anchorage, Alaska, Sept 2000; IEEE: 2000; pp 940−943.

(8) Aroutiounian, V.; Petrosyan, S.; Khachatryan, A.; Touryan, K. *J. Appl. Phys.* **2001**, *89*, 2268−2271.

(9) Raffaelle, R. P.; Castro, S. L.; Hepp, A. F.; Bailey, S. G. *Prog. Photovolt. Res. Appl.* **2002**, *10*, 433−439.

(10) Brown, A. S.; Green, M. A.; Corkish, R. P. *Physica E* **2002**, *14*, 121−125.

(11) (a) Huynh, W. U.; Peng, X.; Alivisatos, A. P. *Adv. Mater.* **1999**, *11*, 923−927. (b) Huynh, W. U.; Dittmer, J. J.; Alivisatos, A. P. *Science* **2002**, *295*, 2425−2427.

(12) (a) Arici, E.; Hoppe, H.; Reuning, A.; Sariciftci, N. S.; Meissner, D. CIS Plastic Solar Cells. In *Seventeenth European Photovoltaic Solar Energy Conference Proceedings*, Munich, Germany, 2001; James and James Ltd.: London, 2001. (b) Arici, E.; Sariciftci, N. S.; Meissner, D. *Mol. Cryst. Liq. Cryst.* **2002**, *385*, 249−256.

(13) Grätzel, M. *Prog. Photovolt. Res. Appl.* **2000**, *8*, 171−185.

(14) Wang, Y.; Herron, N. *J. Lumin.* **1996**, *70*, 48−59.

(15) (a) Nozik, A. J. *Annu. Rev. Phys. Chem.* **2001**, *52*, 193−231. (b) Nozik, A. J. *Physica E* **2002**, *14*, 115−120.

(16) (a) Godovsky, D. Y.; Varfolomeev, A. E.; Zaretsky, D. F.; Chandrakanthi, R. L. N.; Kündig, A.; Weder, C.; Caseri, W. *J. Mater. Chem.* **2001**, *11*, 2465−2469. (b) Chandrakanthi, R. L. N.; Careem, M. A. *Thin Solid Films* **2002**, *417*, 51−56.

(17) Marcinkevičius, S.; Leon, R.; Čechavičius, B.; Siegert, J.; Lobo, C.; Magness, B.; Taylor, W. *Physica B* **2002**, *314*, 203−206.

(18) Walters R. J.; Summers, G. P.; Messenger, S. R.; Freundlich, A.; Monier, C.; Newman, F. *Prog. Photovolt. Res. Appl.* **2000**, *8*, 349−354.

(19) Sobolev, N. A.; Cavaco, A.; Carmo, M. C.; Grundmann, M.; Heinrichsdorff, F.; Bimberg, D. *Phys. Status Solidi B* **2001**, *224*, 93−96.

(20) A search of the term "quantum dot*" in the Science Citation Index in February, 2004 yielded 12 800 hits.

(21) Malik, M. A.; O'Brien, P.; Revaprasadu, N. *Adv. Mater.* **1999**, *11*, 1441−1444.

(22) Czekelius, C.; Hilgendorff, M.; Spanhel, L.; Bedja, I.; Lerch, M.; Müller, G.; Bloeck, U.; Su, D.-S.; Giersig, M. *Adv. Mater.* **1999**, *11*, 643−646.

(23) Gurin, V. S. *Colloids Surf., A* **1998**, *142*, 35−40.

(24) (a) Lu, Q.; Hu, J.; Tang, K.; Qian, Y.; Zhou, G.; Liu, X. *Inorg. Chem.* **2000**, *39*, 1606−1607. (b) Cui, Y.; Ren, J.; Chen, G.; Qian, Y.; Xie, Y. *Chem. Lett.* **2001**, 236−237. (c) Jiang, Y.; Wu, Y.; Yuan, S.; Xie, B.; Zhang, S.; Qian, Y. *J. Mater. Res.* **2001**, *16*, 2805−2809.

(25) Gurinovich, L. I.; Gurin, V. S.; Ivanov, V. A.; Bodnar, I. V.; Molochko, A. P.; Solovej, N. P. *Phys. Status Solidi B* **1998**, *208*, 533−540.

(26) Malyarevich, A. M.; Yumashev, K. V.; Posnov, N. N.; Mikhailov, V. P.; Gurin, V. S.; Prokopenko, V. B.; Alexeenko, A. A.; Melnichenko, I. M. *J. Appl. Phys.* **2000**, *87*, 212−216.

(27) Jiang, Y.; Wu, Y.; Mo, X.; Yu, W.; Xie, Y.; Qian, Y. *Inorg. Chem.* **2000**, *39*, 2964−2965.

(28) (a) Xiao, J.; Xie, Y.; Xiong, Y.; Tang, R.; Qian, Y. *J. Mater. Chem.* **2001**, *11*, 1417−1420. (b) Xiao, J.; Xie, Y.; Tang, R.; Qian, Y. *J. Solid State Chem.* **2001**, *161*, 179−183. (c) Li, B.; Xie, Y.; Huang, J.; Qian, Y. *Adv. Mater.* **1999**, *11*, 1456−1459.

(29) Mandale, A. B.; Sathaye, S. D.; Patil, K. R. *Mater. Lett.* **2002**, *55*, 30−33.

(30) For reviews of this topic see: Murray, C. B.; Kagan, C. R.; Bawendi, M. G. *Annu. Rev. Mater. Sci.* **2000**, *30*, 545−610. Trindade, T.; O'Brien, P.; Pickett, N. L. *Chem. Mater.* **2001**, *13*, 3843−3858.

(31) (a) Trindade, T.; O'Brien, P. *Adv. Mater.* **1996**, *8*, 161. (b) Trindade, T.; O'Brien, P.; Zhang, X. *Chem. Mater.* **1997**, *9*, 523−530. (c) Malik, M. A.; Revaprasadu, N.; O'Brien, P. *Chem. Mater.* **2001**, *13*, 913−920.

(32) Cumberland, S. L.; Hanif, K. M.; Javier, A.; Khitrov, G. A.; Strouse, G. F.; Woessner, S. M.; Yun, C. S. *Chem. Mater.* **2002**, *14*, 1576−1584.

(33) (a) Banger, K. K.; Cowen, J.; Hepp, A. F. *Chem. Mater.* **2001**, *13*, 3827−3829. (b) Banger, K. K.; Harris, J. D.; Cowen, J. E.; Hepp, A. F. *Thin Solid Films* **2002**, *403*−*404*, 390−395. (c) Banger, K. K.; Hollingsworth, J. A.; Harris, J. D.; Cowen, J.; Buhro, W. E.; Hepp, A. F. *Appl. Organomet. Chem.* **2002**, *16*, 617−627. (d) Banger, K. K.; Jin, M. H.-C.; Harris, J. D.; Fanwick, P. E.; Hepp, A. F. *Inorg. Chem.* **2003**, *42*, 7713−7715.

(34) Henderson, D. O.; Mu, R.; Ueda, A.; Wu, M. H.; Gordon, E. M.; Tung, Y. S.; Huang, M.; Keay, J.; Feldman, L. C.; Hollingsworth, J. A.; Buhro, W. E.; Harris, J. D.; Hepp, A. F.; Raffaelle, R. P. *Mater. Des.* **2001**, *22*, 585−589.

(35) Raffaelle, R. P.; Potdevin, T.; Hepp, A. F.; Bailey, S. G. *Mater. Sci., Semicon. Proc.* **1999**, *2*, 289−296.

(36) Hollingsworth, J. A.; Hepp, A. F.; Buhro, W. E. *Chem. Vap. Dep.* **1999**, *5*, 105−109.

(37) Hirpo, W.; Dhingra, S.; Sutorik, A. C.; Kanatzidis, M. G. *J. Am. Chem. Soc.* **1993**, *115*, 1597−1599.

(38) Castro, S. L.; Bailey, S. G.; Raffaelle, R. P.; Banger, K. K.; Hepp, A. F. *Chem. Mater.* **2003**, *15*, 3142−3147.

(39) Peng, X.; Wickham, J.; Alivisatos, A. P. *J. Am. Chem. Soc.* **1998**, *120*, 5343−5344.

(40) Tu, H.; Chikan, V.; Kelley, D. F. *J. Phys. Chem. B* **2003**, *107*, 10389−10397.

(41) Murray, C. B.; Norris, D. J.; Bawendi, M. G. *J. Am. Chem. Soc.* **1993**, *115*, 8706−8715.

(42) (a) Yu, W. W.; Peng, X. *Angew. Chem., Int. Ed.* **2002**, *41*, 2368−2371. (b) Qu, L.; Peng, Z. A.; Peng, X. *Nano Lett.* **2001**, *1*, 333−337.

(43) Talapin, D. V.; Rogach, A. L.; Kornowski, A.; Haase, M.; Weller, H. *Nano Lett.* **2001**, *1*, 207−211.

(44) Mićić, O. I.; Cheong, H. M.; Fu, H.; Zunger, A.; Sprague, J. R.; Mascarenhas, A.; Nozik, A. J. *J. Phys. Chem. B* **1997**, *101*, 4904−4912.

(45) Kuno, M.; Lee, J. K.; Dabbousi, B. O.; Mikulec, F. V.; Bawendi, M. G. *J. Chem. Phys.* **1997**, *106*, 9869−9882.

(46) Dabbousi, B. O.; Rodriguez-Viejo, J.; Mikulec, F. V.; Heine, J. R.; Mattoussi, H.; Ober, R.; Jensen, K. F.; Bawendi, M. G. *J. Phys. Chem. B* **1997**, *101*, 9463−9675.

(47) Peng, X.; Schlamp, M. C.; Kadavanich, A. V.; Alivisatos, A. P. *J. Am. Chem. Soc.* **1997**, *119*, 7019−7029.

(48) Yoshino, K.; Ikari, T.; Shirakata, S.; Miyake, H.; Hiramatsu, K. *Appl. Phys. Lett.* **2001**, *78*, 742−744.

(49) (a) Wakita, K.; Fujita, F.; Yamamoto, N. *J. Appl. Phys.* **2001**, *90*, 1292−1296. (b) Wakita, K.; Hirooka, H.; Yasuda, S.; Fujita, F.; Yamamoto, N. *J. Appl. Phys.* **1998**, *83*, 443−447.

(50) Binsma, J. J. M.; Giling, L. J.; Bloem, J. *J. Lumin.* **1982**, *27*, 55−72.

(51) Binsma, J. J. M.; Giling, L. J.; Bloem, J. *J. Lumin.* **1982**, *27*, 35−53.

(52) Ueng, H. Y.; Hwang, H. L. *J. Phys. Chem. Solids* **1989**, *50*, 1297−1305.